Evolution of the transport properties of fractures subject to thermally and mechanically activated mineral alteration and redistribution

I. FAORO[1,2,3], D. ELSWORTH[2] AND T. CANDELA[3,4]

[1]Department of Earth Sciences, University of Durham, Durham, UK; [2]Department of Energy and Mineral Engineering, G[3] Center and the EMS Energy Institute, Pennsylvania State University, University Park, PA, USA; [3]Department of Geosciences, G[3] Center and the EMS Energy Institute, Pennsylvania State University, University Park, PA, USA; [4]Department of Earth and Planetary Sciences, University of California, Santa Cruz, CA, USA

ABSTRACT

Strong feedbacks link temperature (T), hydrologic flow (H), mechanical deformation (M), and chemical alteration (C) in fractured rock. These processes are interconnected as one process affects the initiation and progress of another. Dissolution and precipitation of minerals are affected by temperature and stress, and can result in significant changes in permeability and solute transport characteristics. Understanding these couplings is important for oil, gas, and geothermal reservoir engineering, for CO2 sequestration, and for waste disposal in underground repositories and reservoirs. To experimentally investigate the interactions between THMC processes in a naturally stressed fracture, we report on heated (25°C up to 150°C) flow-through experiments on fractured core samples of Westerly granite. These experiments examine the influence of thermally and mechanically activated dissolution of minerals on the mechanical (stress/strain) and transport (permeability) responses of fractures. The evolutions of the permeability and relative hydraulic aperture of the fracture are recorded as thermal and stress conditions' change during the experiments. Furthermore, the efflux of dissolved mineral mass is measured periodically and provides a record of the net mass removal, which is correlated with observed changes in relative hydraulic fracture aperture. During the experiments, a significant variation of the effluent fluid chemistry is observed and the fracture shows large changes in permeability to the changing conditions both in stress and in temperature. We argue that at low temperature and high stresses, mechanical crushing of the asperities and the production of gouge explain the permeability decrease although most of the permeability is recoverable as the stress is released. While at high temperature, the permeability changes are governed by mechanical deformation as well as chemical processes, in particular, we infer dissolution of minerals adjacent to the fracture and precipitation of kaolinite.

Key words: kaolinite, matter dissolution, permeability, stress, temperature

Received 15 December 2014; accepted 29 August 2015

Corresponding author: Igor Faoro, Department of Earth Sciences, University of Durham, South Road, Durham, DH1 3LE, UK.
Email: Igor.Faoro@conocophillips.com. Tel: +1-918-661-6806. Fax: +1-918-661-0691.

INTRODUCTION

During last several decades, intense research has been performed on the processes that link temperature (T), hydrologic flow (H), mechanical deformation (M), and chemical alteration (C) in fractured rock (e.g., Tsang 1987; Stephansson *et al.* 1996; Baghbanan & Jing 2008; Faoro *et al.* 2013). These processes are strongly interconnected as one process affects the initiation and progress of another. The evolution of the transport and mechanical properties of rock fractures cannot be predicted by only considering each process independently. These complex coupled behaviors are important in many systems related to oil, gas, and geothermal reservoir engineering and for waste disposal in underground repositories and reservoirs.

It has been observed, for example, that chemical precipitation from aqueous solutions can reduce (Lowell *et al.*

1993) and even completely occlude (Martin & Lowell 2000) rock permeability, transforming open fractures into mineralized veins (Vermilye & Scholz 1995). Thermal expansion or contraction also drastically affects permeability distribution and fluid-flow characteristics (Lowell & Germanovich 1995; Germanovich *et al.* 2000, 2001), including the role of thermal stresses and the nonlinear closure characteristics of fractures to applied stress (Jones 1975; Gangi 1978; Kranz *et al.* 1979; Neuzil & Tracy 1981; Tsang & Witherspoon 1981; Walsh 1981; Raven & Gale 1985; Gavrilenko & Gueguen 1989).

The hydraulic transmissivity of fractured rock masses is strongly affected by coupled THMC processes and is conditioned by the interaction of the evolution of stress, variation of temperature, and the chemistry of the circulating fluid. It remains difficult to predict the response of the fracture (opening or closing) to these processes. During flow-through tests in limestone (Polak *et al.* 2003) and novaculite (Yasuhara *et al.* 2006), for example, spontaneous variations of permeability were recorded in response to changes of temperature without change in stress or of fluid influent chemistry.

To investigate the interactions between THMC processes in a natural stressed fracture, we report on heated flow-through experiments on cylindrical specimens of Westerly granite split by a single fracture parallel to the core axis. During the experiments, the evolution of the hydraulic responses of the fracture (permeability and relative hydraulic aperture) to the imposed changes of the stresses and of the temperatures of the circulating fluid is followed. Furthermore, the efflux of dissolved mineral mass is measured periodically to provide a record of the net mass removal of minerals and to correlate this with the observed hydraulic responses of the fracture during the flow experiment.

EXPERIMENTAL SETUP

The schematic of the experimental setup is represented in Fig. 1a. In a standard triaxial cell within the Temco core holder, a jacketed fractured core sample is placed between two axial cylindrical platens, which is in turn connected to two high-precision pressure syringe pumps operated in stress control mode (pumps type: ISCO 500D, pressure range: 1–70 MPa; for more technical details, refer to Wang *et al.* 2013). The first intensifier applies an identical radial (confining) and axial stress to the cylindrical sample; the second pressurizes the circulating fluid within the sample. The pressure transducers PDCR 610 and Omega PX302-5KGV (resolution of 0.03 MPa) measure, respectively, the pressures of the confining and of the circulating fluid.

The sample comprises a Westerly granite core 25.4 mm in diameter and 100 mm in length that is longitudinally notched to a depth of 2 mm, split in half in a knife-edged de-

vice (see Fig. 1b), cleaned with compressed air, and finally reassembled without offsetting the walls of the fracture.

The sample is first placed between the two cylindrical platens and then jacketed with a PVC sheath (thickness 5 mm). Once the sample is arranged within the Temco pressure vessel, we apply first the confining pressure and then connect the internal hydraulic circuit for fluid injection into and out of the sample.

The inlet fluid (deionized water) circulates in through the upstream fracture edge, transits the sample along the fracture, and drains from the downstream fracture edge. In each experiment, periodic measurements of efflux of dissolved mineral mass provide a record of the net mass removal of constituent minerals.

We perform experiments at different temperatures of the circulating fluid. The Temco vessel is encased within a homemade furnace, and heat is generated by two 'Omegalux' radiant ceramic heater plates (power of up to 2KW and surface temperatures of up to 980°C/1800°F) (see Fig. 1c,d).

In order to minimize the thermal dispersion and to insulate the furnace itself from the heat, the internal walls are lined with sheets of refractory ceramics (thickness: 15 mm) (see Fig. 1d). The temperature of the furnace is controlled by a thermostat to an accuracy of 0.1°C and measured by one thermocouple to an accuracy of 0.01°C. The fluid inlet pipeline to the fracture is long (60 cm) and coiled to guarantee that the inlet fluid is brought to the same equilibrium temperature as the air in the furnace before injection. The significant thermal mass of this coiled line also damps out thermal fluctuations and their effect on thermal expansion of the water.

EXPERIMENTAL PROCEDURE

We report on three deionized water flow-through experiments on three fractured cores of Westerly Granite, and at three different boundary conditions (see Table 1, section: '*Test conditions*').

In the first experiment, performed at room temperature, the stress applied at isotropic condition ($\sigma_1 = \sigma_2 = \sigma_3$) is stepped up and down from 1.5 to 60 MPa, while the pore pressure is adjusted between 150 KPa and 5 MPa to guarantee the continuous circulation of fluid (see Table 1 for details).

In the second experiment, the isotropic stress is kept constant at 5 MPa, and the pressure of the circulating fluid is 150 KPa, while its temperature is stepped up to 150°C and back to 25°C as follows: 25–45, 45–90, 90–120, 120–150, 150–75, and 75–25°C.

Finally, in the third experiment, the isotropic stress is 40 MPa, the pressure of the circulating fluid is adjusted between 1 MPa and 5 MPa, and the fluid temperature is stepped up to 140°C and back to ambient condition as follows: 25–50, 50–100, 100–140, 140–100, and 100–25°C.
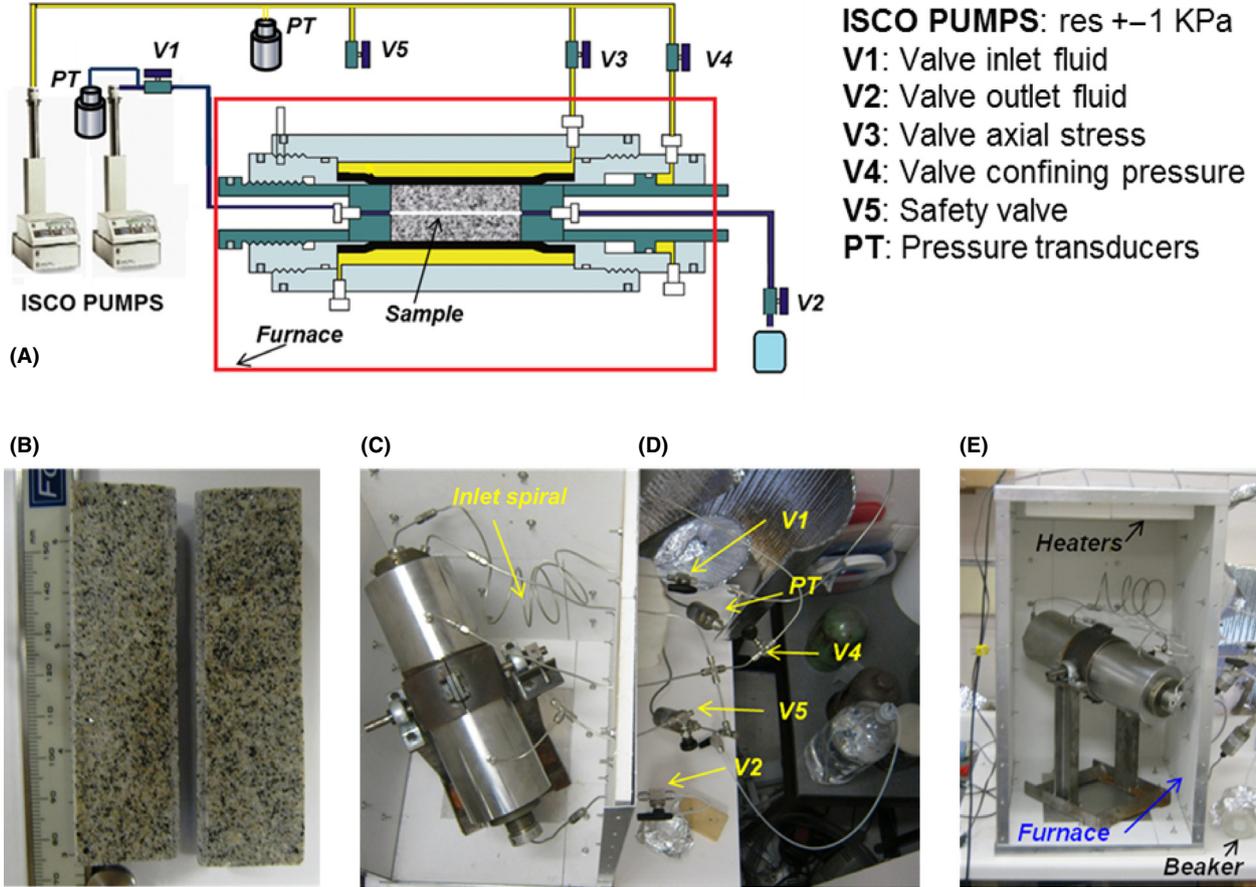
Fig. 1. Equipmental arrangement showing: (*Top* A) the schematic of the pressure vessel, the pressure intensifiers, the plumbing arrangement, and the furnace. In detail: the internal geometry of the pressure vessel with sample (shown in jacket) and the fluid access lines. (*Bottom B*): Westerly granite sample: Φ: 25.4 mm and L:100 mm. (*Bottom C and D*): respectively, the plain and frontal views of the pressure vessel, the plumbing arrangement, and the furnace.

During the experiments, the pumps pressurize both the confining and the circulating fluid, and are operated in stress control mode. Readings of flow rate are continuously recorded. The maximum values of both temperatures and pressures are set according to the limits of the equipment.

In all the experiments, each 'step-like change' of the boundary conditions: Both the stress and the temperature last on an average of ~24 h.

Finally, net effluxes of dissolved mineral mass are measured periodically to provide a record of the net mass removal, which will be ultimately correlated with the changes in aperture observed during the flow test.

RESULTS

The permeability is computed by the measurement of the flow rate at steady-state conditions of stress and temperatures using the following equation:

$$k = \frac{Q \cdot \mu_{(T)} \cdot L_S}{A_S \cdot \Delta h \cdot \rho \cdot g} \tag{1}$$

where k: permeability [m^2]; Q: steady fluid flow rate [m^3 sec^{-1}]; L_S: length of the sample [m]; A_S: cross-sectional area of the sample [m^2]; Δh: water head drop [m]; ρ: water density [kg m^{-3}]; g: gravitational acceleration [m sec^{-2}]; and $\mu_{(T)}$: dynamic viscosity as a function of the circulating fluid temperature: [kg m^{-1} sec^{-1}] (Dortmund Data Bank, *viscosity*):

$$\mu_{(T)} = A \cdot 10^{B/(T-C)} \tag{2}$$

where A: 2.414*10^{-5} [kg m^{-1} sec^{-1}]; B: 247.8 [°K]; C: 140 [°K]; and T: inlet fluid temperature [°K].

The equivalent hydraulic aperture: b is related to the recorded flow rate: Q and the head drop: Δh, measured over the sample of length, L_S, and diameter D_S as:

$$Q = \frac{b^3 \cdot D_S \cdot \Delta h}{12 \cdot \mu_{(T)} \cdot L_S} \tag{3}$$

Finally, the dissolved mineral mass removed (labeled: **Mass** in Table 1) is computed by multiplying the volume

Table 1 Experiments: variables and results.

| Test conditions			Test measurements									
Temp., °C	$\sigma_1, \sigma_2, \sigma_3$, MPa	ΔPore pressure, KPa	k, m²	b, mm	Al, ppm	Ca, ppm	K, ppm	Mg, ppm	Na, ppm	Si, ppm	Volume, ml	Mass, mg
25	1.5	150	2.87e-15	0.189		2.35	0.99	0.22	1.38	0.21	50	0.26
	5	150	1.65e-15	0.157	0.02	1.81	0.35	0.14	0.41	0.19	7.46	0.28
	10	150	1.62e-15	0.156		1.33	0.30	0.12	0.55	0.09	63.53	0.43
	20	150	1.09e-15	0.137		1.02	0.15	0.09	0.14	0.07	25.85	0.47
	40	5000	2.29e-16	0.081	0.15	26.3	1.50	2.78	6.79	1.54	5.43	0.68
	60	5000	1.68e-18	0.015	0.12	52.4	1.79	5.18	14.6	2.25	6.62	1.18
	40	1500	1.08e-18	0.010	0.05	34.3	1.75	3.23	14.5	2.44	4.38	1.43
	20	200	4.42e-19	0.013	0.01	2.58	0.16	0.21	0.96	0.23	11.76	1.48
	10	200	2.29e-16	0.081		0.42	0.09	0.04	0.08	0.06	45.97	1.51
	5	200	1.12e-15	0.138		0.37	0.05	0.03		0.05	60.6	1.54
25	5	150	1.07e-15	0.135		1.57	0.26	0.14	0.73	0.20	65.87	0.19
45			8.09e-16	0.127	0.02	3.30	0.30	0.28	1.69	0.36	33.56	0.39
90			3.46e-16	0.097	0.05	4.47	0.75	0.27	2.37	3.29	71.34	1.18
120			3.45e-16	0.090	0.01	0.80	0.15	0.04	0.34	2.15	45.31	1.34
150			2.04e-16	0.084				0.01		43.1	36.78	2.92
75			2.74e-16	0.093	0.01	0.78	0.78	0.03	1.17	15.3	2.07	2.96
25			9.99e-16	0.126	0.02	2.82	0.22	0.11	0.60	3.82	30.19	3.19
25	40	1000	3.52e-17	0.043	0.06	13.9	0.91	1.46	4.77	0.83	40.27	0.88
50		5000	9.37e-18	0.028	0.08	12.3	0.70	1.08	4.05	1.34	38.96	1.64
100		5000	4.83e-18	0.022	0.10	5.24	0.52	0.32	2.26	3.68	23.65	1.92
140		5000	2.79e-18	0.018	0.03	0.71	0.40	0.02	1.73	34.6	23.87	2.82
100		5000	2.34e-18	0.017	0.01	0.37	0.21	0.01	0.66	22.8	10.07	3.06
25		5000	2.88e-18	0.018	0.14	8.29	8.00	0.18	32.3	14.1	12.57	3.85

of the discharged flow rate (labeled: *Volume* in Table 1) by the aqueous concentrations of the major elements present in the effluent fluid. Initial solid state composition of Westerly granite core is as follows: 27% quartz: SiO_2, 36% microcline: $KAlSi_3O_8$, 30% plagioclase: $NaAlSi_3O_8$ to $CaAl_2Si_2O_8$, and 6% phyllosilicates: $Mg_4Si_6O_{15}(OH)_2 \cdot 6 H_2O$ (Meredith & Atkinnson 1985).

The panel in Fig. 2 shows on the left the evolutions of the permeability as a function of the confining stress for the specimen tested at 25°C and as a function of the temperatures of the circulating fluid for the samples confined, respectively, at 5 MPa and at 40 MPa. On the right of Fig. 2, it is displayed the evolutions of the cumulative dissolved mass removal within the sample as a function of the equivalent hydraulic aperture. The measured magnitudes are reported in Table 1, section: '*Test measurements*'.

The experiment performed at 25°C (top panel, left column Fig. 2) shows that the permeability of the fractured sample is inversely proportional to the confining stress. In this experiment, the sample is loaded from 1.5 to 60 MPa and then unloaded to 5 MPa. The permeability drops by 3 orders of magnitude from the initial value of 2.87e-15 m² to 1.08e-18 m², before recovering to 1.12e-15 m² as the stress is released. The minimum value of permeability is recorded at the first step of the unloading sequence: 40 MPa; the final value is recorded at 5 MPa and is approximately equivalent to that recorded at the same stress during the loading phase: 1.65e-15 m² (see Table 1). The equivalent hydraulic aperture is inferred

from the permeability measurements and therefore follows a similar trend: from 185 μm at 1.5 MPa to 10 μm at 40 MPa (of the unloading phase) and then back to 138 μm at 5 MPa. During this test, 1.54 mgs of mineral mass are removed by dissolution, in particular the largest fraction (~1 mg) at the highest stress, during the loading interval: 40-60-40 MPa (top panel, right column of Fig. 2).

In the heated (150°C) test at the lower constant confining stress (5 MPa), the temperature of the circulating fluid is increased to 150°C before falling to the initial standard conditions: 25°C. The permeability (central panel, left column of Fig. 2) is inversely correlated to the temperature: from an initial value of 1.07e-15 m² at 25°C to a similar final one of 9.99e-16 m² (at the same temperature) after dropping to 2.04e-16 m² at 150°C. The corresponding hydraulic aperture follows the trend of the permeability: 135 μm at 25°C, then a minimum value of 84 μm at 150°C, and finally recovering to a final value of 126 μm. During this test, the amount of dissolved mass is 3.19 mg. At equivalent intervals of time (24 h), 15% (0.5 mg) of the mass has been dissolved between 45 and 90°C and 45% (1.5 mg) between 120 and 150°C (central panel, right column Fig. 2).

Finally, in the heated test (140°C) at the higher confining pressure (40 MPa), the permeability decreases quasi-exponentially from the initial value of 3.52e-17 m² to 2.88e-18 m² although the temperature of the inlet fluid is increased up to 140°C and then cooled to 25°C (bottom
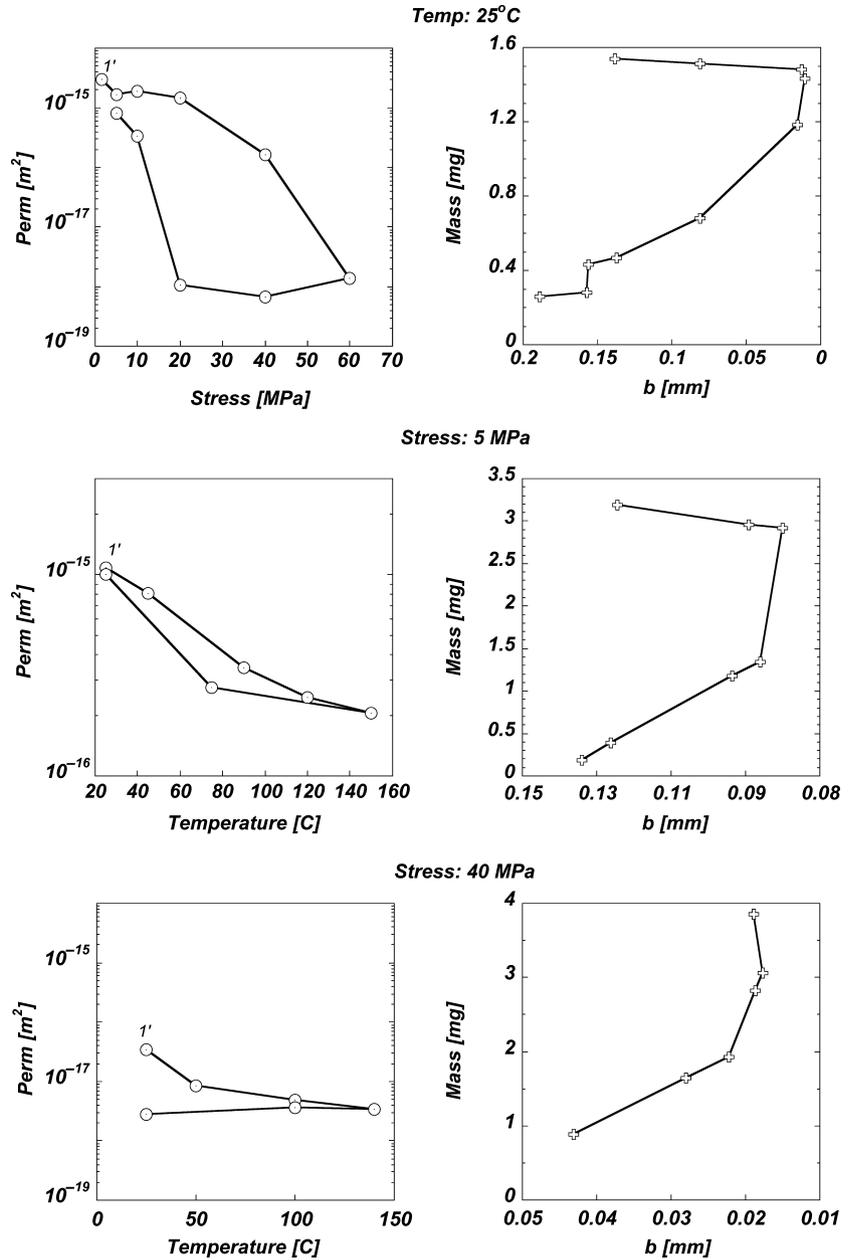
Fig. 2. (*top raw*) For the specimen tested at room temperature, (*left*) evolution of the permeability as a function of confining pressure; (*right*) evolution of the cumulative dissolved mass removed within the sample as a function of the hydraulic aperture: ***b***. For the samples confined, respectively, at 5 MPa (*central raw*) and at 40 MPa (*bottom raw*), evolutions of the permeability as a function of the circulating fluid temperatures (*left*); (*right*) evolutions of the cumulative dissolved mass removed within the sample as a function of the hydraulic aperture: ***b***. These values are also reported in Table 1 in the section: 'Test measurements'.

panel, left column of Fig. 2). The inferred hydraulic aperture reduces from 43 μm to 18 μm following the permeability trend. During this test, 3.85 mgs of dissolved mass were collected, 25% of that between the interval 100–140°C (bottom panel, right column of Fig. 2).

The aqueous concentrations of the main elements (Al, Ca, K, Mg, Na, Si) as a function of applied stress for the sample tested at room temperature (i.e., 25°C) and as a function of the temperatures of the inlet fluid for the samples confined at 5 MPa and 40 MPa are represented in Fig. 3 and reported in Table 1 in the section 'Test measurements'.

Concentrations of the main elements falling below the detection limits of the Perkin-Elmer Optima 5300—Inductively Coupled Plasma Atomic Emission Spectrometry (ICP-AES) are not shown in the figures or in the tables.

In the experiment performed at 25°C (left panel of Fig. 3), we record that for all the elements, the resulting aqueous concentrations exhibit similar trends but different magnitudes: Those of Ca and Na are on average 1 order of magnitude larger than those for Mg, K, and Si and 3 orders of magnitude higher than those for Al. Furthermore, the concentrations are highly sensitive to changes in confining stress. More specifically, the higher the stress,
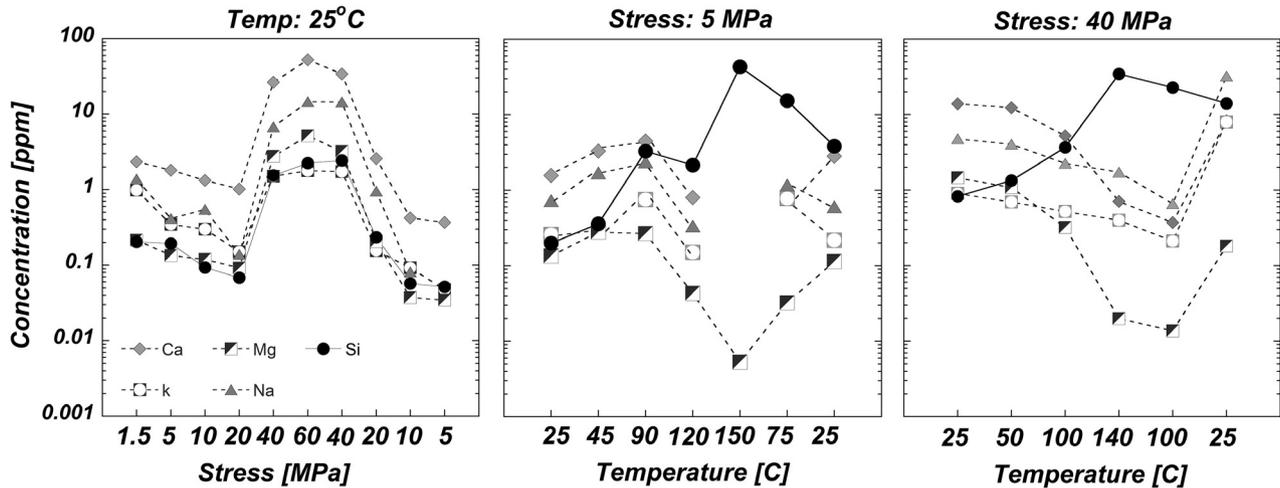
Fig. 3. Concentrations of the main elements (Al, Ca, K, Mg, Na, Si) as a function of the stress for the sample tested at room temperature (*left panel*) and as a function of the temperatures of the inlet fluid for the samples confined at 5 MPa (*central panel*) and 40 MPa (*right panel*). These values are also reported in Table 1 in the section: '*Test measurements*'. Measurements below detection limits are omitted.

the higher the concentrations, except for the initial increase in stress (from 1.5 MPa to 20 MPa) where they decrease slightly. The minimum values are recorded at the end of the experiment when the confining stress is returned to 5 MPa.

For the heated experiment (150°C) confined at 5 MPa (central panel of Fig. 3), the concentrations of each element vary with the temperatures as previously noted, except for the Si which follows an opposite trend after 120C. In more details, between 25°C and 90°C, the higher is the temperature, the higher are the concentrations. The most abundant elements are Ca and Na, followed by Si (that increases of 1 order of magnitude between 45°C and 90°C), then K and Mg, and finally the least abundant is Al (for the entire test, it ranges on average 1 or 2 orders lower that the others: between 0.01 ppm and 0.05 ppm). Between 90°C and 120°C, the concentrations slightly decrease; at 150°C (except Si), they drop to their minimum and then (except Si) increase again to the final values recorded as the temperature is lowered to 25°C. These final values are similar to those measured for the same boundary conditions at the beginning of the test. In contrast, at 150°C the concentration of Si increases ~20 times the previous value at 120°C and reaches its peak of 43.1 ppm; then, during the cooling stage of the experiment, it decreases to its final value of 3.82 ppm at 25°C (~20 times higher than the initial concentration recorded at room temperature).

In the heated experiment (140°C) confined at 40 MPa (right panel of Fig. 3) the concentrations of all the elements are still strongly dependent on the temperature, and except for Si, they follow the same trend. Only the Si, in fact, shows that the concentration is positively correlated

to the temperature of the circulating fluid (the higher the temperature, the higher the concentrations). For all the other elements, this is not true and in fact, their concentrations continuously decrease until the 100°C of the cooling phase where they reach their minimum values (~0.5 times lower than the respective initial concentrations). Then, during the last part of the experiment, at temperatures between 100°C and 25°C, all the concentrations increase to reach their peak values (Na, K, AL) or a value similar to their initial concentration (Ca).

ANALYSIS

Our measurements show that the variations in the stress and the temperature of the circulating fluids affect the hydraulic (permeability), mechanical (hydraulic aperture), and transport (net mass of removal and relative aqueous concentrations of the main elements) properties of the fractures in the Westerly granite samples.

To understand which mechanisms are responsible for the observed results, for each test, we (i) first analyze and correlate the permeability evolutions (Fig. 2) with the development of the aqueous concentrations of the principal elements present in the Westerly granite (Fig. 3), and then, (ii) we compare the rates of hydraulic aperture reduction db/dt_{Hyd} independently computed from equation 3, with the rates (db/dt_{Che}) derived from the recorded effluent concentrations (Fig. 4).

The chemical rates of aperture reduction are calculated as (Polak *et al.* 2003):

$$\frac{db}{dt_{Che}} = \frac{QC_p}{A_c\rho} \qquad (4)$$
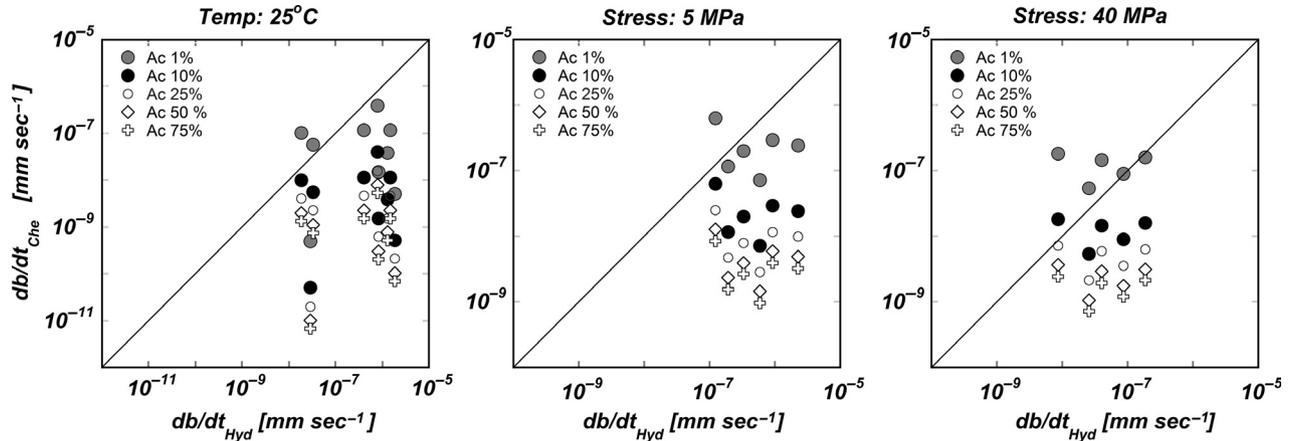
Fig. 4. Comparison between the rates of hydraulic aperture reduction db/dt_{Hyd} and the chemical rates of aperture reduction (db/dt_{Che}).

where Q: steady fluid flow rate [m^3 sec^{-1}]; A_c: fractional contact area of the fracture surfaces [m^2]; C_p and ρ: are, respectively, the concentrations (see Table 2) and the densities of the elements present in the effluent [kg m^{-3}]: 2700 kg m^{-3} for Al, 1550 kg m^{-3} for Ca, 890 kg m^{-3} for K, 1740 kg m^{-3} for Mg, 968 kg m^{-3} for Na, and 2650 kg m^{-3} for Si.

The data represented in Fig. 4 show the chemical aperture rates (db/dt_{Che}) at five different estimated fractional contact areas: 1, 10, 25, 50, and 75%.

From the first test performed at room temperature, we have observed that the permeability is inversely correlated to the applied stress and that the variation of stress does not produce a permanent change in the hydraulic properties of the fracture. At the beginning and end of the experiment, the stress conditions are identical and the initial and final values of the permeability are almost the same. For this test, a fractional contact area of the fracture of 1–10% is needed for the chemical aperture rates to match the hydraulic aperture reduction inferred from permeability measurements (left panel of Fig. 4). This can be explained if we consider that even if the increments of confining stress forcing the progressive mechanical closure of the fracture induce some damage to the contacting asperities,

most of the resulting deformation is recoverable. During the loading path, the creation of gouge temporarily plugs the fracture and reduces the permeability. On the contrary, during the unloading part of the experiment, the relaxation of the stress not only reduces the production of gouge but also facilitates gaping of the fracture and as a consequence, the permeability recovers to close to its initial value at the beginning of the test. This is also confirmed by the fact that, for all the cations, the aqueous concentrations increase as the level of stress becomes higher, namely when the production of gouge is maximum (~1 mg between the stress interval 40-60-40 MPa). In contrast, the concentrations decrease when the production of wear products is absent or at least greatly reduced, that is, precisely at the beginning of the test at stresses below 20 MPa (0.2 mg) and in the second part of the load cycle at stresses ranging between 60 MPa and 5 MPa (0.1 mg).

During the second experiment at a confining stress of 5 MPa, we observe that the changes of permeability depend on the temperature of the circulating fluid and that they are reversible. At this low stress level, the production of gouge by mechanical crushing of the asperities can be considered insignificant: The computed fractional contact area of the asperities is 1% (center panel of Fig. 4). Nonetheless, we have recorded that the production of mass

Table 2 Possible Westerly granite chemical reactions in nonsaturated solutions of distilled water and stoichiometric computations of the weight ratios of the products with SiO_2.

Stoichiometry reactions	** SiO_2	** Ca^{2+}	** Na^+	** K^+	** Mg^+	* Kaolinite * $Al_2Si_2O_5(OH)_4$
$Mg_4Si_6O_{15}(OH)_2 \cdot 6H_2O + 8H^+ \rightarrow 4Mg^{2+} + 6SiO_2 + 11H_2O$	6				4	
$CaAl_2Si_2O_8 + 2H^+ + H_2O \rightarrow Al_2Si_2O_5(OH)_4 + Ca^{2+}$		1				1
$2NaAlSi_3O_8 + 2H^+ + H_2O \rightarrow Al_2Si_2O_5(OH)_4 + 4SiO_2 + 2Na^+$	4		2			1
$2KAlSi_3O_8 + 2H^+ + H_2O \rightarrow Al_2Si_2O_5(OH)_4 + 4SiO_2 + 2K^+$	4			2		1
moles:	14	1	2	2	4	3
molecular weight of 1 mole [g mole^{-1}]:	60.85	40	23	39.1	24.3	258.134
total weight of the moles [g]:	851.9	40	46	78.2	97.2	774.402
ratio SiO_2/** in weight:	1	21.3	18.5	10.9	8.8	1.1

is double than that recorded during the experiment conducted at room temperature (see Table 1 and the bottom panel in the central column of Fig. 2). This result is probably due to the fact that during this test, the most active processes are those of temperature-assisted chemical dissolution of the fracture surface followed by convective transport of the removed material. The mechanism of temperature-assisted chemical dissolution explains the higher productions of mass (bottom panel, central column of Fig. 2) that occurs during the higher increments of temperature (45–90°C and 120–150°C), but is not sufficient to fully explain the permeability behavior. Considering that at higher temperatures, more material is dissolved from the walls of the fracture thus enhancing the fracture permeability, we still need to explain why the permeability decreases with an increase in temperature (especially between 90°C and 150°C) instead of increasing. We find the answer in analyzing how the concentrations of the main elements evolve during the test (central panel of Fig. 3). In particular, we notice that at higher temperatures (90–150°C), the aqueous concentrations (except for Si) decrease, or more precisely, suggesting that the elements such as Ca, Na Mg, and K are consumed, while Si is still produced. That suggests that at higher temperatures, some chemical reactions are likely engaged in forming new material. Such reactions are staunched as the temperatures drop; in fact, the concentrations of the elements that previously were consumed now increase, while the production of Si is reduced. The formation of new material by itself is still not sufficient to explain why the permeability decreases. In order to affect the permeability of the fracture, the new material has to precipitate and clog the fracture. Our analysis, presented in more detail later, favors the formation of kaolinites as the clay mineral could clog the fracture aperture and explain our observations. During the cooling part of the test, the permeability of the fracture increases and regains the same levels recorded at the beginnings of the experiment, because the formation of new material no longer occurs, and instead, the only processes still active are mineral dissolution followed by the transport of the dissolved mass.

Finally, we argue that during the heated test (140°C) at higher stress (40 MPa), the permeability continuously decreases even if the amount of collected mass is the highest (~4 mg), because the processes involved in this experiment are both mechanical (crushing of the asperities due to the high level of stress resulting in an estimated fractional contact area of the walls of the fracture ranging between 1% and 10% [right panel of Fig. 4]) and chemical (formation, precipitation, transport of gouge). If we consider that the values of the recorded mass of this test are the results of the effects of the two mechanisms, we should be able to compare at least the first value: 0.88 mg at 40 MPa and at 25°C, with those of the previous experiments that were recorded under similar boundary condi-

tions. In particular, the value from the first experiment (0.68 mg at 40 MPa and at 25°C) should represent the mechanical part, while the value from the second test (0.19 mg at 25°C) should be related to the chemical effect (values are reported in Table 1). Their summation is 0.87 mg, which is in agreement with the value of the mass (0.88 mg) recorded during this test. Furthermore, considering the evolution of the concentrations (right panel of Fig. 3), we can immediately recognize that those chemical reactions (previously detected in the heated experiment at 5 MPa), consuming most of the Na, Ca, Mg, and K and producing Si, are progressing as the temperatures rise during the experiment. As it happens for the previous experiment, we assume that the newly formed material precipitates, clogs the fracture, and reduces its permeability. We infer that as the temperatures drop, the production of the new mineral halts and the permeability increases. In this case, the increment of permeability recovery is small and the permeability does not reach values similar to the initial magnitudes because the stress is high, and the processes of dissolution and transport of material are slower.

This new material that is formed during the heated parts of the experiments could be kaolinite ($Al_2Si_2O_5(OH)_4$), produced from the reactions of dissociation in water of both the plagioclase and the microcline present in the granite. In general, the possible chemical reactions that are developed from the Westerly granite in unsaturated solutions of distilled water are as follows:

for the phyllosilicates:

$$Mg_4Si_6O_{15}(OH)_2 \bullet 6H_2O + 8H^+ \rightarrow 4Mg^{2+} \\ + 6SiO_2 + 11H_2O \tag{5}$$

for the plagioclase:

$$CaAl_2Si_2O_8 + 2H^+ + H_2O \rightarrow Al_2Si_2O_5(OH)_4 + Ca^{2+} \tag{6}$$

for the plagioclase:

$$2NaAlSi_3O_8 + 2H^+ + H_2O \rightarrow Al_2Si_2O_5(OH)_4 \\ + 4SiO_2 + 2Na^+ \tag{7}$$

for the microcline:

$$2KAlSi_3O_8 + 2H^+ + H_2O \rightarrow Al_2Si_2O_5(OH)_4 \\ + 4SiO_2 + 2K^+ \tag{8}$$
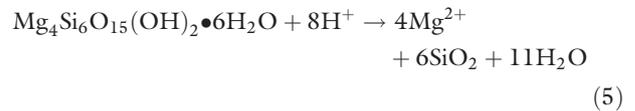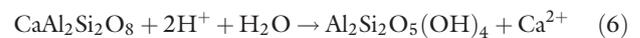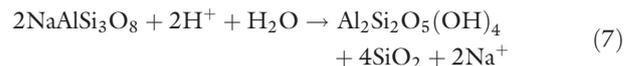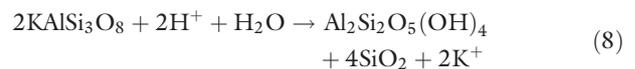
For each element (see Table 2), we first compute the total stoichiometric weight of the moles produced from the reactions and then we calculate its weight ratio with the SiO_2 (those raw values are reported in Table 2 as labeled: '*ratio SiO_2/** in weight*'). It is important to compare the stoichiometric, theoretical weight ratios of the SiO_2 with the experimentally measured ratios. We assume, in fact, that the reactions (5,6,7,8) occur and that the kaolinite is formed when the experimental weight ratios

Table 3 Mass removal and experimental computations of the weight ratios of the main elements with SiO_2.

| Test conditions		Test measurements								
Temp., °C	$\sigma_1, \sigma_2, \sigma_3$, MPa	Ca, μg	K, μg	Mg, μg	Na, μg	Si, μg	$\frac{Si}{Na}$	$\frac{Si}{Mg}$	$\frac{Si}{K}$	$\frac{Si}{Ca}$
25	1.5	117.46	49.43	10.77	69.16	10.27	0.148	0.953	0.208	0.087
	5	13.52	2.59	1.01	3.08	1.44	0.469	1.430	0.558	0.107
	10	84.46	19.05	7.63	34.71	5.95	0.171	0.779	0.312	0.070
	20	26.33	3.91	2.38	3.61	1.77	0.490	0.743	0.453	0.067
	40	142.95	8.17	15.11	36.87	8.36	0.227	0.554	1.024	0.059
	60	346.64	11.84	34.30	96.55	14.90	0.154	0.434	1.258	0.043
	40	150.04	7.65	14.13	63.31	10.70	0.169	0.757	1.398	0.071
	20	30.35	1.84	2.42	11.27	2.76	0.245	1.141	1.499	0.091
	10	19.39	4.27	1.71	3.76	2.63	0.700	1.534	0.616	0.136
	5	22.38	2.89	2.10		3.13		1.491	1.082	0.140
25	5	103.59	17.06	8.91	48.07	13.09	0.272	1.469	0.767	0.126
45		110.90	9.91	9.38	56.87	12.07	0.212	1.288	1.218	0.109
90		318.93	53.52	18.98	168.91	234.64	1.389	12.365	4.384	0.736
120		36.42	6.81	1.95	15.22	97.36	6.395	49.856	14.287	2.673
150				0.19		1584.99		8130.906		
75		1.62	1.61	0.07	2.42	31.77	13.111	475.180	19.718	19.584
25		85.00	6.56	3.43	18.24	115.36	6.324	33.608	17.585	1.357
25	40	559.33	36.44	58.84	191.99	33.33	0.174	0.566	0.915	0.060
50		480.79	27.12	42.18	157.85	52.18	0.331	1.237	1.924	0.109
100		123.94	12.35	7.57	53.53	87.12	1.627	11.504	7.051	0.703
140		16.91	9.50	0.48	41.33	825.81	19.983	1738.497	86.947	48.837
100		3.75	2.13	0.14	6.66	229.89	34.521	1666.350	108.041	61.385
25		104.22	100.50	2.28	405.84	176.99	0.436	77.579	1.761	1.698

values are larger than the stoichiometric ones. We calculate the experimental values from the records of the aqueous concentrations of the main elements. For each test, those values are reported in Table 3 and are represented in Fig. 5. In particular, in Fig. 5, the stoichiometric values (that vary between 1 and 21.3) are highlighted in the '*stoichiometric range box*'.

Those results are consistent with all previous assumptions. In fact, for the first test in which we assume that only mechanical processes occur, the experimental ratios are below the stoichiometric range (left panel of Fig. 5), while for the heated tests, during the heating part of the experiments, precisely after 90°C at 5 MPa and 100°C at 40 MPa, they become equal or larger than the theoretical range. Those values also persist higher than the theoretical range during the cooling phase of the tests. Consequently, the precipitation of kaolinites, a process dominant at higher temperatures, is then replaced at lower temperatures by the chemical dissolution of the fracture surface and the transport of the dissolved material.
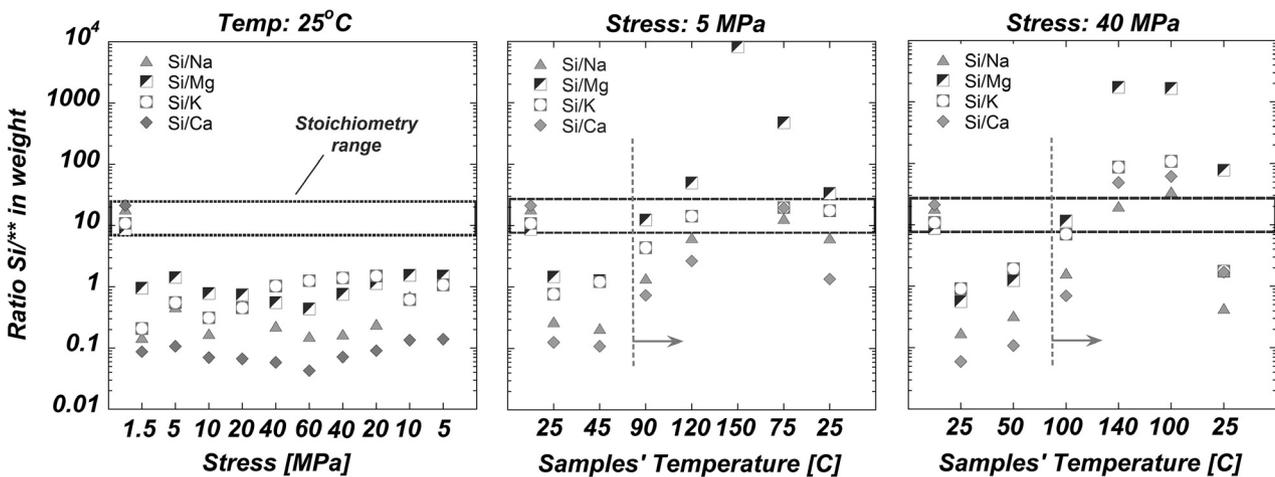
Fig. 5. Comparison between the theoretical/stoichiometric and the experimental weight ratios of the main elements with SiO2 as a function of stress for the sample tested at room temperature (*left panel*) and as a function of the temperatures of the inlet fluid for the samples confined at 5 MPa (*central panel*) and 40 MPa (*right panel*). These values are also reported in Table 3 in the section: '*Test measurements*'.

Westerly granite: Pristine sample
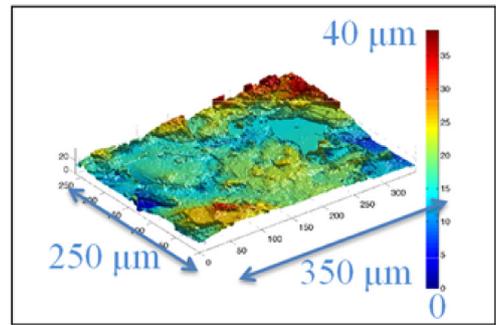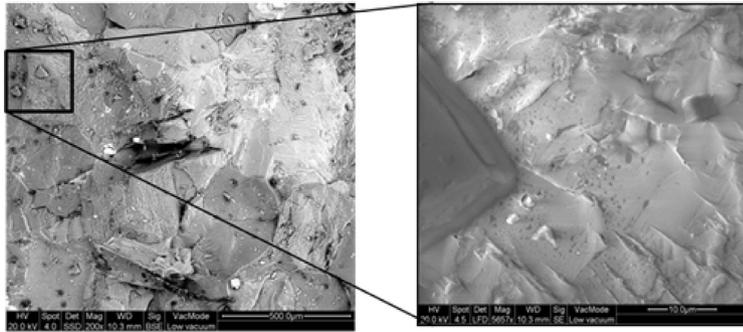
Westerly granite: Stress 5 MPa
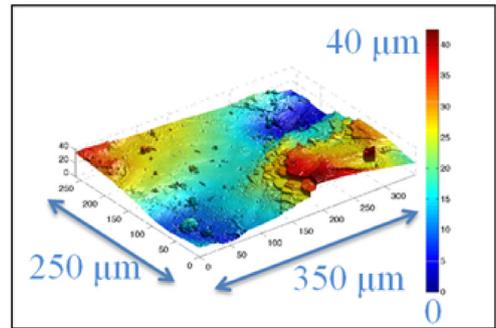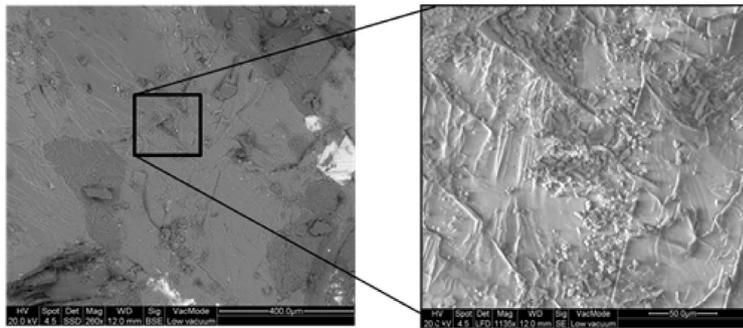
Westerly granite: Stress 40 MPa
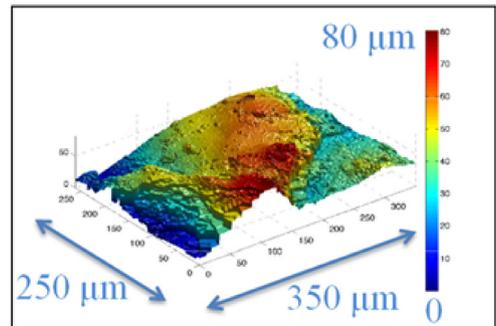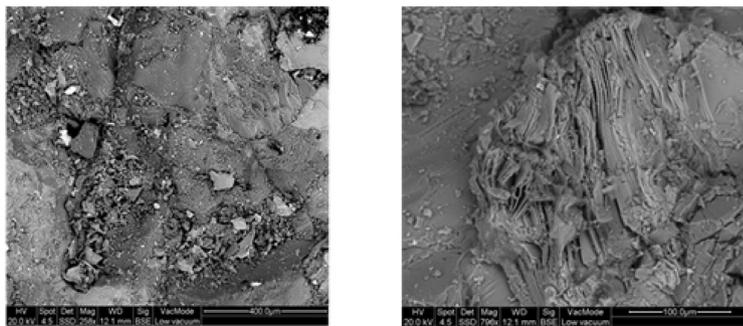
Fig. 6. Analysis using scanning electron microscopy including estimations of the roughness of the fractures via white light interferometry on surfaces of the following: (*top*) pristine sample of Westerly granite; (*center*) sample heated to 150°C confined at 5 MPa; and (*bottom*) sample heated to 140°C confined at 40 MPa.

We have sought physical evidence of the presence of kaolinite in our heated samples. On the two heated samples and on one fracture of pristine Westerly granite, we have completed scanning electron microscopy (SEM) analysis and estimates of the roughness of the fractures via white light interferometry (Candela *et al.* 2012). The results are reported in Fig. 6. A detectable trace of kaolinite has yet to be found, but the roughness and SEM measurements show that the fracture surface is relatively cleaner, rougher, and with angular crystal before the experiments compared to after the heated test at 5 MPa where the surface appears slightly altered, coated with fine particles, and smoother. Finally, the signs of heavy alteration and chemical transformations become more evident on the surface of the heated sample loaded at higher stresses.

Although promoted by the development of damage within the fracture in response to changes in effective stress, this evolution of permeability is similar in nature to the evolution of impermeable caprocks in geothermal reservoirs. The mechanism noted here is specific to fractures, but this initial reduction in permeability could be the precursor to the evolution of convection cells that then promote large-scale recirculation of fluids that then underplate the initial barrier.

CONCLUSION

In order to experimentally investigate and to contribute to better understand the interactions between THMC processes in a natural stressed fracture, we have performed three flow-through experiments on fractured cylindrical cores of Westerly granite, measuring continuously the evolution of hydraulic (permeability and relative hydraulic aperture) and the transport (records of aqueous concentration and net mass of removal) responses of the fractures as the conditions of stress and temperature of the circulating fluid changed during the experiments.

In particular, we argue that the reversible changes of the permeability (from 2.87e-15 m^2 to 1.08e-18 m^2 and back to 1.12e-15 m^2) recorded during the first test (performed at room temperature on a sample cyclically stressed up to 60 MPa) are essentially due to mechanical effects of damaging of the asperities of the walls of the fracture. In particular, we think that at higher stresses, the permeability is reduced because crushed fine materials temporary clog the fracture, while as the stress relaxes, the permeability continuously increases (reaching values similar to the ones recorded at the beginning of the test) because the mechanical crushing stops and most of the deformation is recoverable.

From the second test, in which the confining stress is kept constant at 5 MPa as the temperature of the injecting fluid rises from 25°C up to 150°C, by analyzing the distribution of the aqueous concentrations of the main elements, we demonstrate that the initial reduction in the permeability (from 1.07e-15 m^2 at 25°C to 2.04e-16 m^2 at 150°C) could be due to the formation of the kaolinite, while the subsequent increase (up to initial values) as the temperatures lower is mainly due to the process of chemical dissolution of the fracture surfaces associated with the transport of the dissolved matter. During the unloading path, transport of the newly formed kaolinites could also explain their absence along the fracture plane at the end of the experiment.

Finally, in the last experiment (the fracture is tested at constant stress of 40 MPa in a temperature cycle from 25°C to 140°C), the continuous decrease in the permeability from 3.52e-17 m^2 to 2.34e-18 m^2 is probably due to the fact both the mechanical and the chemical mechanisms, described above, occur simultaneously.

These experiments have implications for the long-term evolution of permeability in hydrothermal and EGS-type geothermal systems. As noted above, the mechanically induced damage may serve as a precursor to small-scale fracture-based reduction in permeability that may first initiate the sealing of a caprock above hydrothermal systems. This initial reduction in permeability would be the trigger to allow the deepening of the caprock with the resulting formation of convective circulation cells below.

However, the mechanism is more likely of importance in EGS-type systems that are directly analogous to these experiments—fractures are created in either Mode I or II, have fresh and reactive surfaces, and cycle through a number of stress states during multistage stimulation and then production. Under these circumstances, the significant loss of permeability that may result due to hydrothermal alteration is an important consideration in the loss of function of such conduits for flow and heat transfer. The time scale of these effects is rapid and would be important on time scales of both stimulation and production.

ACKNOWLEDGEMENTS

REFERENCES

Baghbanan A, Jing L (2008) Stress effects on permeability in fractured rock masses with correlated fracture length and aperture. *International Journal of Rock Mechanics and Mining Sciences*, **45**, 1320–34.

Candela T, Renard F, Klinger Y, Mair K, Schmittbuhl J, Brodsky EE (2012) Roughness of fault surfaces over nine decades of length scales. *Journal of Geophysical Research*, **117**, 8409. doi:10.1029/2011JB009041.

Dortmund Data Bank: http://www.saylor.org/site/wp-content/uploads/2011/04/Viscosity.pdf

Faoro I, Vinciguerra S, Marone C, Elsworth D, Schubnel A (2013) Linking permeability to crack density evolution in thermally stressed rocks under cyclic loading. *Geophysical Research Letters*, **40**, 2590–5.

Gangi AF (1978) Variation of whole and fractured porous rock permeability with confining pressure. *International Journal of Rock Mechanics and Mineral Science-Geomechanics Abstracts*, **15**, 249–57.

Gavrilenko P, Gueguen Y (1989) Pressure dependence of permeability: a model for cracked rocks. *Geophysical Journal International*, **98**, 159–72.

Germanovich LN, Lowell RP, Astakhov DK (2000) Stress dependent permeability and the formation of seafloor event plumes. *Journal of Geophysical Research*, **105**, 8341–54.

Germanovich LN, Lowell RP, Astakhov DK (2001) Temperature-dependent permeability and bifurcations in hydrothermal flow. *Journal of Geophysical Research*, **106**, 473–95.

Jones FO (1975) A laboratory study of the effects of confining pressure on flow and storage capacity in carbonate rocks. *Journal of Petroleum Technology*, **1975**, 21–7.

Kranz RL, Frankel AD, Engelder T, Scholz CH (1979) The permeability of whole and jointed Barre granite. *International Journal of Rock Mechanics and Mineral Science- Geomechanics Abstracts*, **16**, 225–35.

Lowell RP, Germanovich LN (1995) Dike injection and the formation of megaplumes at ocean ridges. *Science*, **267**, 1804–7.

Lowell RP, Van Cappellen P, Germanovich LN (1993) Silica precipitation in fractures and the evolution of permeability in hydrothermal upflow zones. *Science*, **260**, 192–4.

Martin JT, Lowell RP (2000) Precipitation of quartz during high temperature fracture-controlled hydrothermal upflow at ocean ridges: equilibrium versus linear kinetics. *Journal of Geophysical Research*, **105**, 869–82.

Meredith PG, Atkinnson BK (1985) Fracture toughness and subcritical crack growth during high temperature tensile deformation of Westerly granite and Black gabbro. *Physics of the Earth and Planetary Interiors*, **39**, 33–51.

Neuzil CE, Tracy JV (1981) Flow through fractures. *Water Resources Research*, **17**, 191–9.

Polak A, Elsworth D, Yasuhara H, Grader AS, Halleck PM (2003) Permeability reduction of a natural fracture under net dissolution by hydrothermal fluids. *Geophysical Research Letters*, **30**, doi:10.1029/2003GL017575.

Raven KG, Gale JE (1985) Water flow in a natural rock fracture as a function of stress and sample size. *International Journal of Rock Mechanics and Mineral Science- Geomechanics Abstracts*, **22**, 251–61.

Stephansson O, Jing L, Tsang CF (1996) *Coupled Thermo-Hydro-Mechanical Processes of Fractured Media*. Elsevier Science V, Amsterdam.

Tsang CF (1987) *Coupled Processes Associated with Nuclear Waste Repositories*. Academic Press, San Diego.

Tsang YW, Witherspoon PA (1981) Hydromechanical behavior of a deformable rock fracture subject to normal stress. *Journal of Geophysical Research*, **86**, 9287–98.

Vermilye JM, Scholz CH (1995) Relation between vein length and aperture. *Journal of Structural Geology*, **17**, 423–34.

Walsh JB (1981) Effect of pore pressure and confining pressure on fracture permeability. *International Journal of Rock Mechanics and Mineral Science- Geomechanics Abstracts*, **18**, 429–35.

Wang S, Elsworth D, Liu J (2013) Permeability evolution during progressive deformation of intact coal and implications for instability in underground coal seams. *International Journal of Rock Mechanics and Mining Sciences*, **58**, 34–45.

Yasuhara H, Polak A, Mitani Y, Grader A, Halleck P, Elsworth D (2006) Evolution of fracture permeability through fluid-rock reaction under hydrothermal conditions. *Earth and Planet Science Letters*, **244**, 186–200.